Bounding Natural Frequencies in Structures II: Local Geometry, Manufacturing and Preload Effects

William C. Shust, P.E.
Mechanical Engineer
Objective Engineers, Inc.
363 Venturi Dr.
Pueblo West, CO 81007
objengrs@aol.com

Keith B. Smith
Research Engineer
Southwest Research Institute®
6220 Culebra Road
San Antonio, TX
kbsmith@swri.org

ABSTRACT

For two decades, vibration researchers have been improving techniques to precisely measure and predict natural frequencies. For high-risk and high-volume designs, both analysts and experimentalists have welcomed this improved accuracy. However, for the many products of lower risk and/or volume (and therefore smaller development budgets), engineers are often confronted with a question of whether everyday structural issues necessarily require increased detail in test and modeling efforts. And as a further complication, test conductors may not always understand different interpretations and usefulness of modal data as applied to noise, vibration and harshness problems versus those of durability. The first few vibration modes (usually of greater deflection and lesser damping) most often drive most structural fatigue issues, whereas the higher mode shapes can dominate acoustic problems.

The inherent value of precision is examined, as needed in dynamic response prediction or measurement. Dynamic variations exhibited between unique copies of a common design are measured. Variability due to manufacturing repeatability and preloading is examined; differences due to temperature and thermal effects are presented. Knowledge of natural frequency variability helps data consumers to ensure sensible test/analysis requests. Implications of the data highlighted will guide design and test engineers from a variety of industries to more effectively meet the varied needs of their specific clients.

NOMENCLATURE

y	=	out-of-plane deflection of neutral surface
C	=	arbitrary constant (amplitude of steady-state vibration)
$\omega = 2\pi f$	=	circular frequency (f = cyclic frequency)
t	=	time
k	=	wave number
x	=	distance along length of beam
L	=	overall beam length
A	=	area of beam cross section
ρ	=	material density
E	=	Young's modulus
I_z	=	Area moment of inertia about neutral axis of bending/vibration
ε	=	material strain
σ	=	material stress
M	=	applied moment around neutral axis of bending/vibration

h	=	dimension (parallel to y) from neutral axis to outer fiber of beam
$r_z = \sqrt{I_z / A}$	=	radius of gyration about neutral axis of bending/vibration
$V_{\max-\mathrm{mod}}$	=	maximum modal velocity for a given mode shape
$V_{snd-mat} = \sqrt{E/\rho}$	=	longitudinal velocity of sound through material
X_1, X_2	=	constants for beam bending & vibration based on boundary conditions
m	=	normalized mass per unit length of beam
g	=	gravitational acceleration
ζ	=	equivalent viscous damping ratio
ω	=	beam bending natural frequency
$\Delta E/\Delta T$	=	change in Young's Modulus versus temperature
FRF	=	frequency response function, here acceleration response to force input, H_1 technique

BACKGROUND

Research in this field has often focused on the variations in modal parameter results, as affected by the many ways to (a) excite a structure, (b) process the signals, or (c) to curve-fit the FRF data. Conversely, this project examines small variations in modal parameters for reasons often beyond the control of the test engineer: test item variability due to manufacturing differences, assembly differences, surface finish differences, as well as one environmental factor—temperature. Vibrations were created using step relaxation or impacts. For simplicity, the data acquired was analyzed without windowing, only the H_1 FRF formulation, and only half-power or log-decrement damping estimations. It is believed that the conclusions are valid regardless of the simple techniques.

A recurring topic of discussion is the potential payback of a better test and/or modeling effort. For the lower volume ground vehicle industry (commercial, construction vehicles), this balance may be further clouded by additional manufacturing variability. This paper will show the modal repeatability of a structural component design, and therefore indicate a reasonable level of model correlation. The topic herein evolved while fielding questions about modeling mass-produced (commodity) products. For example, "When is my railroad coach model close enough to the first few tested frequencies?" The authors intend this project as the first step toward objective support for our historically subjective answers.

Historically, a rule of thumb for workaday design has remained test/model agreement within 10% for the first several modes, as described over 30 years ago by Hay and Blew [1] as "standard engineering accuracy." As of 1991, Riding and Weeks [2] stated that 5% frequency accuracy on all relevant modes would be "a very good model." However, depending on the application, phrases such as "compares well" may indicate wider discrepancies between test and analysis: as Przybylinski *et al.* [3] referred to a comparison of a 4.28 Hz first bending test mode and a 6.1 Hz model output.

Variability of natural frequencies has been studied extensively with respect to damage detection. Such projects have often investigated behavior of a one-of-a-kind structure, with and without known flaws. For example Cornwell, *et al.* [4] did extensive testing on the Alamosa Canyon highway bridge to examine environment and measurement variations of the first natural frequency. They report 6% variation in modal frequencies over a 24-hour period, correlated to the temperature differential found on the bridge deck. A 95% confidence interval is shown for the first natural frequency, we interpret this as a 0.6% standard deviation due to factors (environmental and measurement) other than the deck temperature differential.

Fewer references were found regarding the similitude of test responses found for nominally identical parts:

- Kompella and Bernhard [5] tested 155 Isuzu chassis for acoustic response to structural and acoustic inputs. They report FRF variations of 4-8 dB between their 40 Hz (low frequency of interest) to 500 Hz. Vehicle-to-vehicle differences are listed as the primary source of variation. Without quantifying, they also state that significant variation (within repeated measurements on reference chassis) was because of environmental and measurement errors.

- Marwala and Hunt [6] tested 22 seam-welded steel cylinders both with and without a fault. For the undamaged population, standard deviations ranging from 0.36-0.75% were found for the first seven experimental natural frequencies. Of the first 16 modes, the 8th resonance showed the greatest variability with a standard deviation of 5%.
- Chen, *et al.* [7] tested 3 reinforced concrete beams in bending, 2 of which were identical. They reported 3.4% difference in first bending modes.
- Lyon [8] cites tests of 88 engines and castings with about an 8dB variation in accelerance FRF magnitudes up to 3200 Hz. Without quantifying, he suggests that the lower 2 to 3 resonance frequencies were "similar" for all structures. He also showed that FRF magnitude variability is inversely related to modal overlap. That is, a population of modally rich structures will exhibit more consistent FRFs than structures with widely spaced modes. Similarly, we expect highly damped structures to show more FRF similarity than lightly damped structures.
- Without quantifying, Migeot [9] *et al.* endorses stochastic FEA techniques to provide meaningful simulations for the variations of individual properties exhibited by several similar structures taken from a production line. He also states that frequency response scatter will increase significantly with frequency.
- Dossing, in a Bruel & Kjaer application note [10] on testing a rapid transit train lists first natural frequencies for four train cars. Both a new and an "old" vehicle of each of two types (2 trailers and 2 coaches built by the same builder) were described as "very similar." The trailers' first bending frequencies differed by 19%, the coaches by 11%. The old vehicles showed higher damping during 1st-bending than new (trailers' damping increased by 38%, the coaches' by 126%).
- McClelland, *et al.* [11] list test data for a highway tractor's first bending mode as 6.5-7.0 Hz. The source of this +/-3.7% variation is unclear.

FOCUS ON LOWEST VIBRATIONAL MODES (RELATIVE MODAL DAMAGE)

This investigation is limited to effects perceived on the two lowest vibration modes in fairly linear test structures. The authors' experience in the fields of structural fatigue and ride quality reflect this frequent importance of the first few to first several modes. The literature also supports this viewpoint. Stein [12] notes that in typical mechanical structures, the dynamic magnification of motion at resonance generally decreases and the damping increases at subsequent (higher frequency) modes. Especially with respect to fatigue, Vold, *et al.* [13] states since strain is a spatial derivative of displacement, not velocity or acceleration, it naturally emphasizes lower frequency data. Finally, per standard ISO-2631 the human perception of ride discomfort is heavily weighted toward 1-2, 4-8, and 10-16 Hz for whole-body lateral, whole-body longitudinal and hand-arm vibration, respectively [14].

Vibration-Induced Fatigue

Traditional crack-initiation approaches to fatigue analysis emphasize the importance of the larger strain cycles in a structural loading history. Even the much debated concept of a crack growth threshold is analogous to this emphasis on damage due to the higher amplitude cycles (*i.e.*, in the implied assumption of zero damage from small cycles). In the increasingly specialized world of structural engineering, where fatigue and modal analysts often work independently, important questions regarding natural frequencies of the greatest interest are often passed over (*e.g.*, which mode shapes drive the most fatigue damage).

Experience has demonstrated that the first few resonant modes of vibration are often the most immediately damaging to primary structure. This is because higher mode shapes are often accompanied by smaller local deflections and consequently less incremental damage (excluding any design-specific effects of substructure resonances on local attachment points, *etc.*). For this reason, modal analysis and testing of many aeronautical, mechanical and civil structures can often be limited to the first few natural frequencies for each major degree of freedom in a system. A conceptual demonstration of why maximum strains drop significantly for the higher modes of vibration is developed here using simple beam theory.

Strain Proportionality to Modal Mach Number

For a semi-infinite beam (*i.e.*, a beam that will accept sinusoidal vibration at all frequencies) where the wavelength of all mode shapes of interest are long compared to the depth of the beam (*i.e.*, neglecting rotational inertia and shear) the governing equation of vibration transverse to its length can be generally stated as [15]:

$$y = C\cos(\omega t)\cos(kx) \qquad \text{where:} \quad k^4 = \omega^2 A\rho / EI_z \tag{1}$$

Assuming bending around the plane of symmetry in this initially straight beam, the deflection curve is also known and can be directly related to strain in the outer fibers as follows [16]:

$$\varepsilon = \frac{\sigma}{E} = -\frac{Mh}{EI_z} = h\frac{\partial^2 y}{\partial x^2} \qquad \text{where:} \quad \varepsilon_{\max} = h\left(\frac{\partial^2 y}{\partial x^2}\right)_{\max} \tag{2}$$

Recalling that maximum strain occurs where the deflection curve is maximized (second spatial derivative of governing displacement equation), and substituting peak modal velocity ($V_{\max-\mathrm{mod}} = -C\omega$) from the first time derivative of the governing displacement equation (1) yields:

$$\varepsilon_{\max} = h(-Ck^2) = h\left(\frac{-C\omega}{\sqrt{I_z/A}\sqrt{E/\rho}}\right) = \left(\frac{h}{r_z}\right)\left(\frac{V_{\max-\mathrm{mod}}}{V_{snd-mat}}\right) \tag{3}$$

Note that the longitudinal velocity of sound is given by the modulus and density of the *material*, while the radius of gyration is given by the area of the *cross section* and its second moment. Thus, the maximum strain for any transverse free vibration mode shape of a beam is proportional to its "modal mach number" [17], or maximum modal velocity divided by the longitudinal speed of sound through the material. In the case of a beam with a constant cross section, the constant of proportionality is based on the cross section and is simply the distance from the neutral axis to the edge of the cross section divided by its radius of gyration.

Higher Modes Exhibit Smaller Strains

For a given beam, the cross-section and material parameters in equation (3) remain constant across mode shapes (*i.e.*, h, r_z & $V_{snd-mat}$ stay the same for different natural frequencies so long as the beam is not physically changed). Therefore, the maximum strain at each increasing natural frequency is simply a function of the maximum modal velocity for each natural frequency. Furthermore, this maximum modal velocity will occur at the antinode with the largest displacement for a particular mode shape.

From general beam theory, the well-known flexural equations for maximum bending displacement and fundamental natural frequency are respectively:

$$y_{\max} = -X_1\left(\frac{mgL^4}{EI_z}\right) \qquad \text{and} \qquad \omega = X_2\sqrt{\frac{EI_z}{mL^4}} \tag{4}$$

Please note that m here is normalized (mass per unit length). The constants X_1 & X_2 are generalized, but are available throughout the literature for various boundary conditions [18-20]. Substituting these into the relationship for peak modal velocity gives:

$$V_{\max-\mathrm{mod}} = -C\omega = -y_{\max}\omega = \left(X_1 X_2 g\sqrt{m/EI_z}\right)\left(L^2\right) \tag{5}$$

And finally, inserting this back into the relationship for maximum strain (3) leaves:

$$\varepsilon_{\max} = \frac{X_1 X_2 hg\sqrt{A\rho m}}{EI_z}\left(L^2\right) \approx CONST_{mat\&geo}\left(L^2\right) \quad (6)$$

Representing the maximum strain formulation through curvature for simple bending displacement and the fundamental mode shape (both have the same shape function under 1-G loading conditions) allows a view of maximum strain as a function of beam length for the first bending mode of vibration.

Simple Application Example: Pinned Ends

The implication of this is most easily demonstrated with a simply supported beam. Here, the second bending mode has a wavelength of half that of the first. Likewise, the third bending mode has a wavelength equal to one-third the total beam length; this pattern is shown schematically in Figure 1.

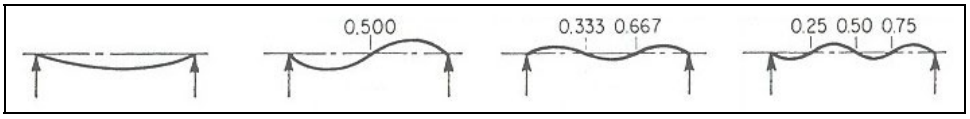

Figure 1. Deflected Shape of Simply-Supported Beam in First Four Bending Modes

It can be assumed that the third mode of this beam is equivalent to three beams (end to end), each one-third the length of the original, each with curvature corresponding to the first bending mode of its truncated length. Using the logic above, the maximum strain associated with each bending mode for a constant base acceleration (*i.e.* equal energy across input bandwidth) can be compared as follows:

$$\frac{(\varepsilon_{\max})_{\text{mod}-2}}{(\varepsilon_{\max})_{\text{mod}-1}} \approx \frac{CONST \times (L/2)^2}{CONST \times (L)^2} = \frac{1}{4} \quad ; \quad \frac{(\varepsilon_{\max})_{\text{mod}-3}}{(\varepsilon_{\max})_{\text{mod}-1}} \approx \frac{CONST \times (L/3)^2}{CONST \times (L)^2} = \frac{1}{9} \quad ; \textit{ etc.}$$

Therefore, for the simply supported beam, the second bending mode has strains that are 0.250x those of the first, the third bending mode has strains that are 0.111x the first, *etc.* The relative maximum strains for this undamped simply-supported beam bending are plotted below in Figure 2.

Notice that the maximum strain in the fourth bending mode is less than 7% that of the first bending mode. In this example, it is likely that only strains due to the first two mode shapes are of interest to the stress analyst, given that fatigue endurance limits are generally about 40% of yield strength for metals.

In complex structures, there are exceptions to this trend such as local stress concentrations that may be located such that they are more sensitive to a higher mode than a lower mode. Also, periodic forcing functions may concentrate energy near a higher mode causing problems before lower frequencies vibrations. Regardless, whether modeling or preparing a test plan, the first few to several modes should receive primary attention.

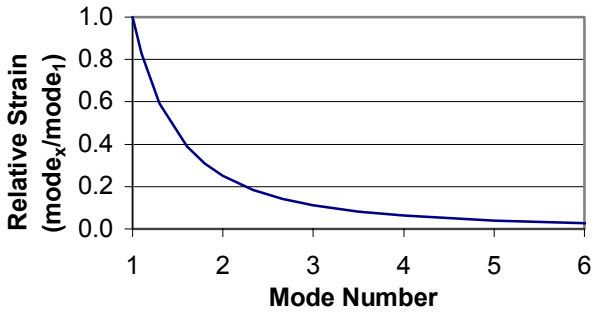

Figure 2. Maximum strain for simply-supported beam at natural bending frequencies.

TEST SEQUENCES OF NOMINALLY SIMILAR STRUCTURES

Test Setup and Data Collection

A search was conducted to find a suitable population of nominally similar but simple structures. The following criteria were desired for the potential test items:

- Nominally identical (same design)
- Manufactured as a structural element (no planning or knowledge as a test coupon)
- Exhibit some measurable manufacturing differences (*e.g.* dimensions)
- Allow for assembly differences (*e.g.* fastener torques)
- Show a range of usage (*e.g.* new vs. old, clean vs. rusted)
- Portable

Several manufacturers were contacted with a request for suitable samples (ranging from full vehicles to small cantilevered brackets), without success. Figure 3 shows two of seven steel brackets that were eventually located at a industrial salvage yard. Each consists of an 8.5 x 3 inch structural c-channel (AISI C3x4.1) fillet arc welded on top of an 11 x 3 x 3/16 inch flat steel bar. All showed mild to aggressive rusting activity and peeling paint. Each specimen was stamped with a unique serial number for tracking purposes. In the balance of this paper, individual specimens will be referred to using their serial number (*e.g.* SN2). Over 30 dimensions were measured on each to quantify spatial variability. Overall length dimensions varied by less than 0.035" (0.3%). The location of the channel along the bar length varied by less than 0.042" (0.8%). Hole pattern centers end-to-end varied by 0.052" (0.65%). The weld fillet legs were nominally 0.23 inches, locally varying by 0.07 inches (30%).

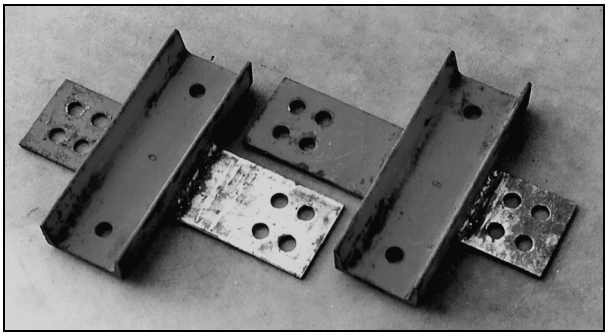

Figure 3a. Two of seven salvaged production weldments before the final test series. The darker locations show the original paint and rust. The shiny areas show the contacting surfaces after stripping paint with a wire brush wheel.

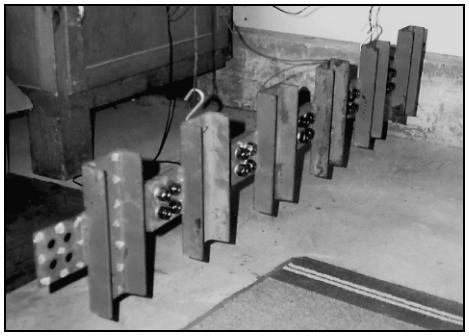

Figure 3b. One of six long-beam assemblies hanging from springs during step-relaxation tests. The short beam series was similar except three weldments were connected back-to-back directly to another three.

Three series of driving point FRF tests were performed using these weldments in free-free conditions:

- Individual weldments. First and second mode differences between the individual weldments
- Long-beam assemblies. First mode differences between long-beam assemblies (6 specimens joined end-to-end)
- Short-beam assemblies. First and second mode differences between short-beam assemblies (3 pairs of specimens joined together and end-to-end)

Although not the primary purpose of this study, a roving force modal survey was made of one weldment. As expected, the first two modes show the flat bar flexing and the much stiffer c-channel acting as a mass (Figure 4). This also provided a good population of consecutive FRFs for the same weldment & test conditions (sampling rate 10kHz, blocksize=64000, 16 ensemble averages, uniform window). Which allowed a statistical analysis of the variation in estimating the fundamental magnitude peak. Using 42 locations, the sample mean for SN7 was found to be 362.811 Hz, with a sample standard deviation of 0.118 Hz (just less than 1 spectral line width of 0.156 Hz). Thus, a +/-3 standard deviation confidence interval around the repeatability of the frequency peak was +/-0.354 Hz (+/-0.98%, or +/-2.8 spectral lines).

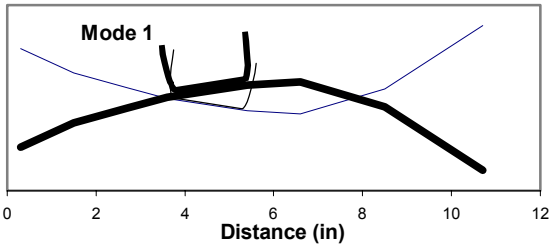

Figure 4a. First bending mode of individual weldment SN7, nominally 363 Hz. C-channel acts mostly as mass.

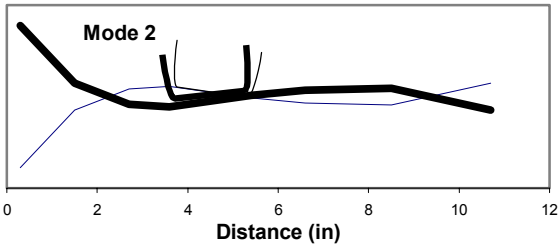

Figure 4b. Second bending mode of individual weldment SN7, nominally 789 Hz.

Certain data collection parameters were held constant for all further tests. The PCB impact hammer was fitted with a plastic tip. Conservatively, this provided sufficient input energy to 1400 Hz (-30dB). The sampling rate was 10 kHz, with AA filters set to 3.3kHz. All rigid body frequencies were verified to be at least 1/10th the first flexible frequencies. Recording and trigger conditions ensured that the entire impulse signal was recorded and saved. Coherence functions were checked against acceptable values of 0.98 and 0.94 respectively, for the first and second modes. These criteria were met for all but a few FRFs (discarded). Figure 5 shows sketches of an individual weldment, the long and short beam assemblies, and force and response directions measured in this study:

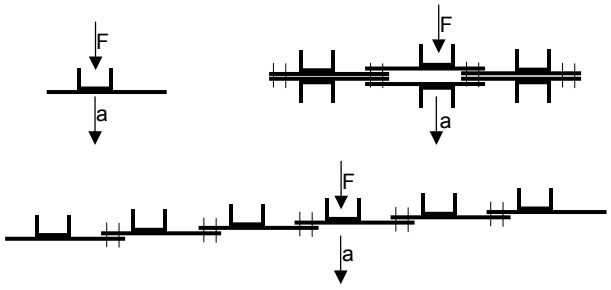

Figure 5. Schematic diagram of weldments, and force & response vectors: individual (left), short beam (right), long beam (bottom).

Individual Weldment Test Series

This series was used to examine part-to-part variation in natural frequency, as well as temperature effects. A block of open-cell upholstery foam was prepared with a clearance hole for the accelerometer, and a traced outline of the weldment to control position on the foam. Driving point accelerance measurements were taken at the centerline intersection on each specimen using a force hammer. Sixteen ensemble averages were collected for 5 of the 7 weldments. A small thermocouple junction was attached near an estimated nodal point for temperature recording.

Figure 6 shows a typical FRF magnitude measurement for an individual weldment. The frequency axis extends to 5kHz due to the 10KHz sampling rate. This seemingly excessive sampling speed was chosen because of the later application of the log-decrement method to the decay. In other words, it was desired that sampling occurred often enough to capture very accurate peak amplitudes of any desired response decay. Again, the first and second bending modes were of interest herein, at about 363 and 789 Hz. Figure 7a shows the raw natural frequencies (estimated as the peaks of the FRF magnitude, subject to 0.156 Hz spectral resolution). As shown, each weldment exhibited a consistent reduction of bending frequency with increasing temperature. Linear slopes were fit to these five data sets, and averaged to yield a new coefficient of (–90.3e-6 / °F). These response versus temperature data indicate that—within a given weldment—the bending natural frequencies can vary just over 1% for a 115°F change. The authors have performed cross-country outdoor testing on large vehicles where surface temperature swings have exceeded this range.

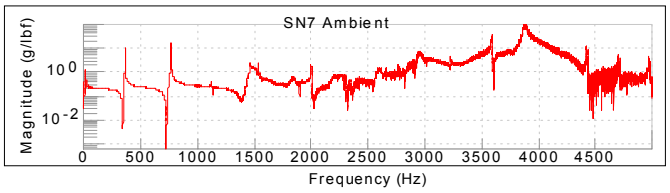

Figure 6. Typical FRF magnitude for individual weldment.

The classical Euler bending beam equation $\{ \omega \sim (EI/mL^4)^{1/2} \}$ shows that free thermal growth in length, height and width change the numerator and denominator equally therefore leaving natural frequency unaltered.

Also, since each mass does not change, this coefficient is believed to reflect the empirical change in Young's Modulus E with respect to temperature. The value of –90e-6 agrees fairly well with a reference [21] found for high-carbon wire listed as –117e-6.

Figure 7b shows the same data, after compensating all natural frequencies (using –90e-6/°F) to their value expected at 70°F. After temperature compensation, the range of weldment natural frequencies is 360.1 to 369.0 Hz (a 2.2% range relative to the mean value).

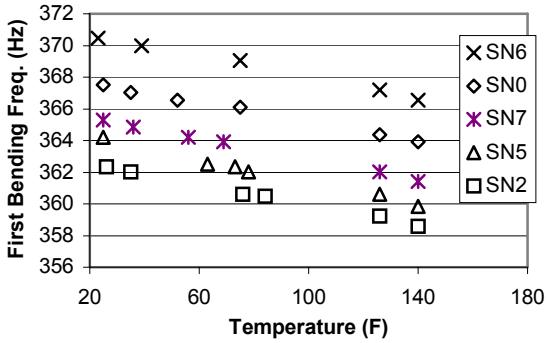

Figure 7a. Raw natural frequencies versus temperature for five individual weldments.

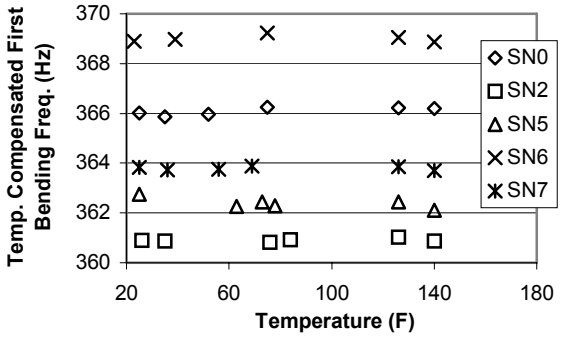

Figure 7b. Temperature-compensated natural frequencies versus temperature for five individual weldments.

Damping values were estimated for the 5 weldments in two ways. Figure 8a shows the results of half-power analyses. These values are rather crude because the bandwidths were found to be just a few spectral lines wide.

Widely spaced modes allowed a second damping estimation technique via the log-decrement method in Figure 8b. A digital bandpass filter was used to remove effects of other modes from the free decay recordings (3-pole Butterworth passing 242-488Hz, nominally 66% and 133% of resonant frequency). Because comparison of just two consecutive cyclic amplitudes can vary, our log decrement calculations used an average of hundreds of such consecutive pairs throughout multiple records. Further details of the method are found in the Appendix. In both figures, the damping values increase roughly 50% as the temperature increased by 115°F. For a given test temperature, the damping estimates for the five weldments had a range of about 30%.

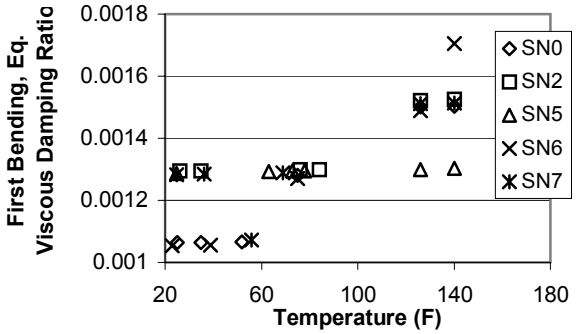

Figure 8a. Damping (via half-power) versus temperature for five individual weldments.

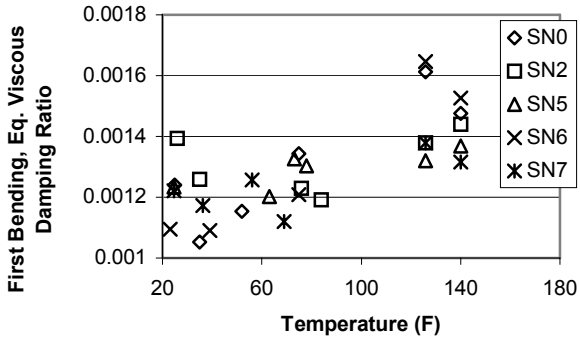

Figure 8b. Damping (via log decrement) versus temperature for five individual weldments.

The natural frequency estimations were repeated for the second bending mode and are shown in Figure 9a & 9b. Again the –90.3e-6 removes the temperature trend. The first two impact tests of weldment SN5 showed natural frequency values about 8Hz higher than the remaining runs. Perhaps the parallel surfaces at the c-channel and plate interface were rusted together until the third thermal or test cycle.

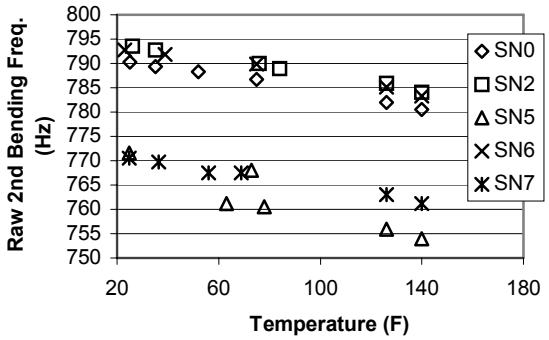

Figure 9a. Raw 2nd natural frequencies versus temperature for five individual weldments.

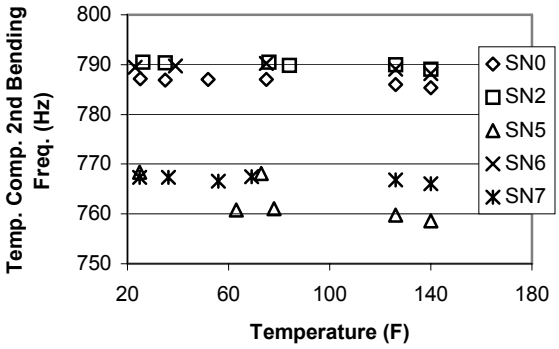

Figure 9b. Temperature-compensated 2nd natural frequencies versus temperature for five individual weldments.

Second-mode damping values were estimated for the 5 weldments using the half-power (or bandwidth) analyses only. Figure 10 shows these rather crude values, having a high versus low range of 66% relative to the midpoint. Overall the values are slightly lower than for the first mode. No trend related to temperature was found.

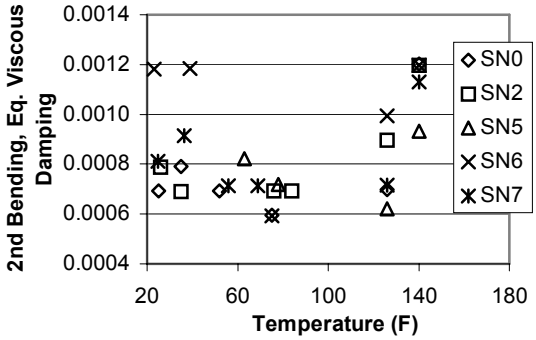

Figure 10. Damping (via half-power) versus temperature for five individual weldments.

Long-beam Test Series

This series was used to examine natural frequency variation of an assembly, as well as temperature effects, but only the first bending mode was investigated. Several 6-weldment beams were assembled by daisy-chaining the 4-hole patterns on the plates (Figure 1b). These were referred to as assembly layouts A through G. A different one of the seven possible weldments was left out of the beam for each assembly. Also, the layout orders (from left end to right end) were randomized such that no weldment occupied the same position twice. Thus, each 84-piece (including fasteners) assembly could be considered as a unique result from a given assembly line.

For beam assemblies A-G, all were pulled lengthwise before snugging the fasteners. This made each as long as possible, given the bolthole clearances. However layout AA used the same serial numbers and weldment order as assembly A, but with the beam pushed lengthwise before tightening. These two layouts were therefore similar except AA was 0.49" shorter (or about 0.9%).

The fasteners fit the holes well at ½" UNC, and Grade 8 strength were chosen to resist wear during the many layout changes. For the first data set, fasteners were torqued by hand to Grade 2 torque values (55 +/-4 lb*ft). Later test torques were limited to Grade 5 to avoid thread damage. Hardened washers were used under bolt heads and nuts.

The beam was hung from two low stiffness steel springs, attached near the first bending nodes. The vibration direction was chosen out-of-plane relative to the support springs for further system decoupling. An accelerometer was placed at midspan. The beam was quasi-statically pushed at the center, pulled on each end, and step-relaxed into (mostly) a first bending mode. Therefore, this test series used single-channel analyses (response only, no FRFs) as shown in Figure 11.

Four such twangs were performed at two different fastener torques. Again, a thermocouple was attached near an estimated nodal point. Shop ambient temperature swings only (30°F) were recorded in this series. Even after accounting for the torque effect found (see below), no trend of damping values over the smaller temperature ranges could be readily identified.

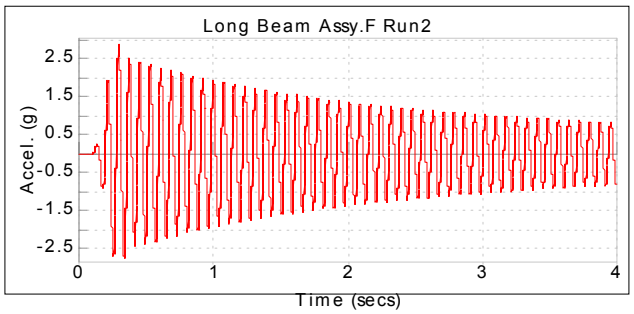

Figure 11. Typical first four seconds of time decay for long beam after step relaxation.

Figure 12a shows the natural frequencies (estimated by timing a several hundred cycles within four beam relaxations. These natural frequencies were also temperature compensated, even though the thermal range required only very small changes. As shown, each beam layout exhibited a bending frequency increase with increasing fastener torque. (Small horizontal shifts of some data points were made on these plots to better differentiate each layout. They do not indicate specific torque variations). The various beams showed lower fundamental bending frequencies for Grade 5 assembly torques (85 +/-4 lb*ft) than for Grade 2 (55 +/-4 lb*ft) by a range of 0.58% to 2.2%. The average of frequency changes for all eight assemblies indicates 1.2% higher overall frequencies for the larger assembly torque than the lower.

Figure 12b shows the damping estimates for the eight long-beams. The various beams showed less damping for Grade 5 assembly torques (85 +/-4 lb*ft) than for Grade 2 (55 +/-4 lb*ft) by a range of 3.8 to 16%. The average of data from all eight layouts indicates 9.8% less overall damping for the higher assembly torque.

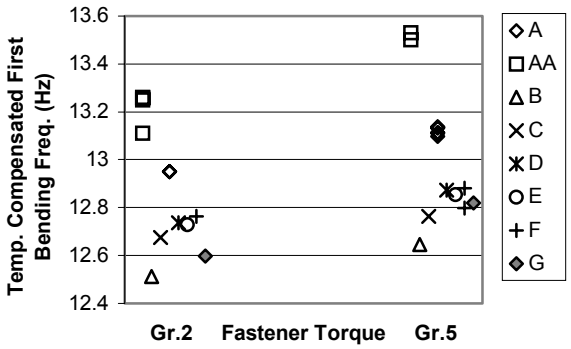

Figure 12a. Temperature-compensated natural frequencies versus fastener torque for eight assemblies.

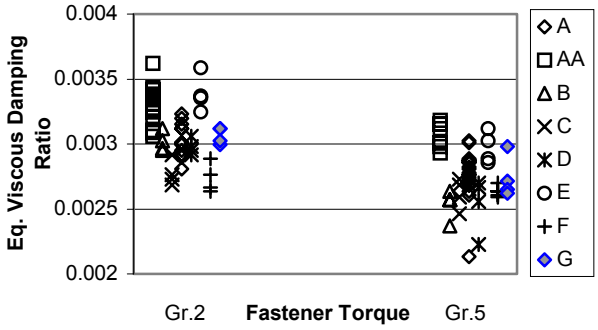

Figure 12b. Damping estimates for eight long-beam assemblies, computed via log-decrement.

Regarding the slightly longer A versus slightly shorter AA results, the shorter beam showed average natural frequencies 2 - 3% larger at both assembly torques. For the length change involved, Euler's beam equation predicts the shorter beam should exhibit a 1.9% higher natural frequency. Thus the A versus AA results are as expected. (The equation predicts the natural frequency ratio for two similar beams of different lengths to be inversely proportional to the ratio of their lengths squared—please see our companion paper [22]). The average damping estimates are about 6% larger for the shorter beam at both torque levels. This may be due to the slightly larger portion of bolted weldment-to-weldment overlap area resulting from the shorter assembly.

Short-beam Test Series

This series was used to examine natural frequency variation of another beam pattern, as well as an added lower assembly torque, and surface finish effects. For the short beams, three weldments were connected back-to-back directly to another three. Thus, each resulting beam was two weldments "thick" and only three long (Figure 5, top right). Due to time constraints only two combinations were attempted, referred to as assemblies A and B. After a first data set was recorded with each beam in its original condition, all mating surfaces were stripped using a rotating steel brush. This allowed for a second data set with fairly clean steel-on-steel surfaces, compared to the

original painted conditions. (Since dimensional and/or mass changes were not desired, the brush removed loose rust but did not remove enough material to return a shiny finish everywhere.)

The two short beam layouts were specially selected based on slight planar curvatures along the 3"x11" steel bars of each item. For the A layout, the convex surfaces were placed so as to minimize weldment back-to-back contact area. For the B layout, the concave surfaces were placed to maximize the back-to-back contact area. Again, each beam could be considered as a unique result from a given assembly line, but not a random selection as in the long-beam series.

Both beams were made as short as possible before tightening, in order to minimize overall length variations due to hole clearances. For the first run, fasteners were torqued by hand to only 25 +/-4 lb*ft (substantial, but below Grade 2 torques). Subsequent runs used the Grade 2 and Grade 5 values as well.

The beams were again hung from two springs, attached near the first bending nodes. An accelerometer was placed at midspan. The beam was too stiff for step-relaxation input, so the impulse hammer was used and FRF functions were measured (Figure 13). Again vibration was out-of-plane relative to the support springs to further decouple the system.

Figure 14a shows the temperature-compensated first bending natural frequencies for the short beams. At all three torques, the scatter indicates 3% variation in first bending frequencies. Both A & B layouts indicate increasing frequency with increasing torque. After combining data from both layouts, an average slope of 0.057 Hz/(lb*ft) was found. Comparing the two higher torques (Grade 2 versus Grade 5), this translates into a 1.7% increase in average first bending frequency (slightly larger than for the long beam series).

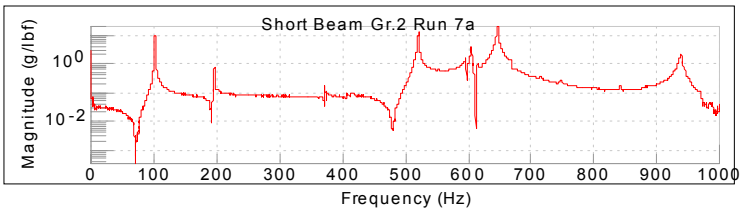

Figure 13. Typical FRF magnitude for short beam.

Figure 14b shows the damping ratios estimated for these two layouts. These estimates were made using the log-decrement method after bandpass filtering the response signals at 66% and 133% of the resonance frequency. Multiple runs within a given test condition agree fairly well. However there is wide scatter across the various conditions, indicating that any trend of damping versus torque was overwhelmed by the assembly difference factor. With all data combined, the stripped runs exhibit 45% less damping than the original surface condition runs. Less damping was expected for the stripped conditions, since the paint could be considered as a very small surface layer damping treatment and since the beam is a step closer to a monolithic structure without layers of paint between the various layers of steel.

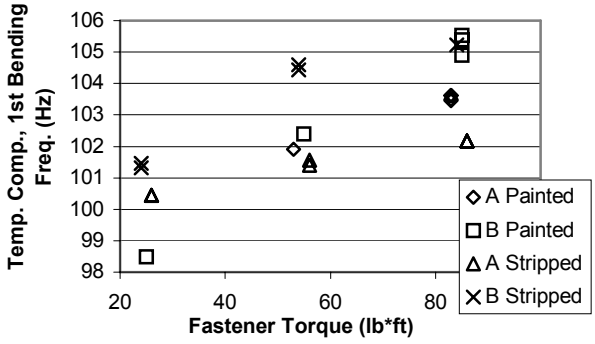

Figure 14a. Temp.-compensated natural frequencies versus fastener torque for two short-beam assemblies.

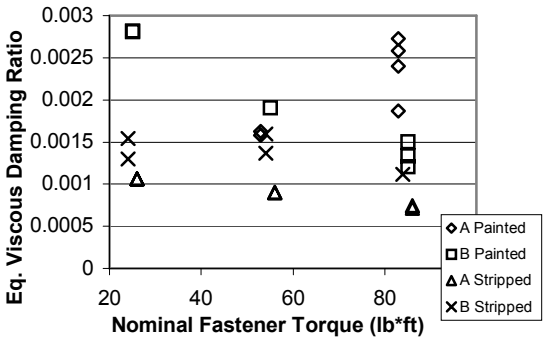

Figure 14b. Damping estimates for two short-beam assemblies, computed via log-decrement.

Second bending natural frequencies are shown in Figure 15a (temperature-compensated) for the short beams. The larger scatter at the low-end torques indicates 7% variation in second bending frequencies. Both layouts indicate increasing frequency with increasing torque. After combining data from both layouts, an average slope of

0.16 Hz/(lb*ft) was found. For the Grade 2 to Grade 5 comparison, this translates into a 2.6% increase in average second bending frequency.

Figure 15b shows the damping ratios estimated for these two layouts. These are again rough values due to use of the half-power method on a too lightly damped mode—an unsatisfactory practice. No trends are apparent. With all data combined, the stripped runs exhibit 5% less damping at the second mode of vibration than found in the original surface condition runs.

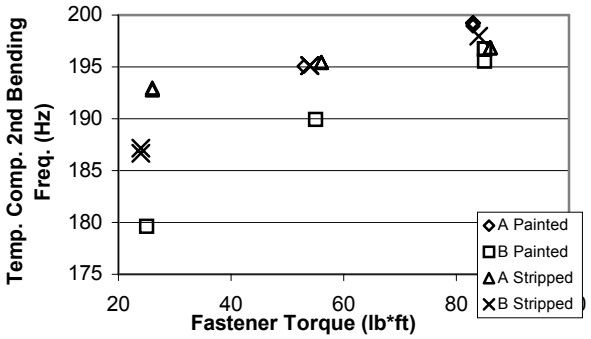

Figure 15a. Temperature-compensated natural frequencies versus fastener torque for eight assemblies.

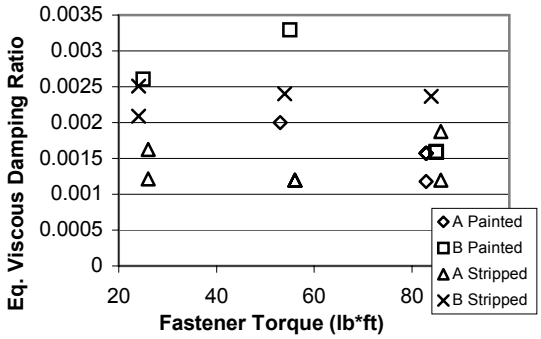

Figure 15b. Second bending mode, damping estimates for two short-beam assemblies, computed via half-power.

STATISTICAL SUMMARIES

During development of these test procedures, several instances of repeated measurements were performed to examine back-to-back repeatability of the parameter estimates. This was not the examination of part-to-part variability, but instead depended more on instrumentation noise and excitation technique. Table 1 shows the confidence bands for natural frequency and damping estimates. Natural frequencies were estimated by the peak found in the FRF magnitude for the single weldment and short beam series, and by cyclic counting for the long beam series. Equivalent viscous damping as reported here was determined from average log decrement readings across several decays. Due to the sharpness of FRF peaks herein, the less accurate half-power method was not investigated for confidence intervals.

Table 1. Variability in consecutive modal parameter estimations deemed due to instrumentation noise and excitation consistency.

Test Series	Confidence Bands for First Mode Estimates from Consecutive Data under Same Conditions			
	Natural Frequency (Hz)		Equiv. Viscous Damping Ratio	
	1-Sigma (95.6%)	3-Sigma (99.7%)	1-Sigma (95.6%)	3-Sigma (99.7%)
Individual Weldment SN7	+/-0.33%	+/-0.98%	+/-1%	+/-3%
Long Beams	+/-0.19%	+/-0.57%	+/-5%	+/-15%
Short Beams	Not examined	Not examined	+/-16%	+/-47%

The various results presented in the data plots 7-15 have been summarized in Table 2. The Young's Modulus variation with temperature, and the shortening of the long beam allowed by bolthole clearances are deemed deterministic because well known equations predict them. The effects of assembly torque changes form a predictable trend, but are not deterministic. The effect of surface finish was reasonable, but not conclusive.

Table 2. Variability in modal parameter estimations due to manufacturing, assembly, and environmental factors.

Test Series	Description of Phenomena	Frequency (Hz)		Equiv. Viscous Damping Ratio	
		Mode 1	**Mode 2**	**Mode 1**	**Mode 2**
Individual Weldments	Nominal Parameter Values	365 Hz	780Hz	0.0013	0.0009*
	Change Due To 115°F Temperature Increase (Deterministic via ΔE/ΔT)	-1.1%	-1.2%	+50%	Inconclusive
	Part-To-Part Parameter Range Among 5 Weldments	**2.2%**	**3.8%**	**27%**	**66%**
Long Beams	Nominal Parameter Values	13 Hz	35 Hz	0.0029	Not Examined
	Change Due To –0.9% Overall Length Change Via Bolt Hole Clearances, A-AA (Deterministic via Euler's Beam Equation)	+2.5%	Not Examined	+6%	Not Examined
	Change Found After Increasing Grade 2 To Grade 5 Fastener Torques	+1.2%	Not Examined	-9.8%	Not Examined
	Part-To-Part Parameter Range Among 7 Random Assemblies, A-G, Within a Torque Category	**6%**	Not Examined	**35%**	Not Examined
Short Beams	Nominal Parameter Values	102	192	0.0016	0.0018*
	Change Found After Increasing Grade 2 To Grade 5 Fastener Torques	+1.7%	+2.6%	No Trend	No Trend
	Part-To-Part Parameter Range Among 2 Selected Assemblies, A-B, Within a Torque Category	**3.1%**	**7%**	**111%**	**78%**
	Change Found After Stripping Paint On Mating Surfaces via Wire Brush Wheel	Inconclusive	Inconclusive	-45%	-5%
					*Larger Uncertainty Due to Half-Power Method

CONCLUSIONS

This study was intended to provide the authors with a better understanding of modal parameter variability. In specific, some often neglected factors caused by manufacturing and assembly procedures have been examined. Although the data acquired was analyzed with the more basic of modal processes, it is believed that the conclusions are valid regardless of the simple techniques.

Various readers will likely pull different information from the two tables above, but several concluding statements have been deemed more important:

- Parameter variations found related to manufacturing, assembly and environmental conditions were orders of magnitude higher than variations due to measurement noise and excitation consistency. This is critical, since its quantification is often overlooked.
- Regardless, whether modeling or preparing a test plan, the first few to several modes should receive primary attention. For random and/or transient environments, the structure will generally experience significantly larger gross operating strains associated with the lower modes than for higher modes.

- Changes in bending natural frequency related to temperature were predicted by the thermal coefficient of Young's modules for carbon steel. This is not the same phenomena described in Cornwell's [4] highway bridge, since that study examined temperature differential.
- Small length changes allowed by bolthole clearances were predictable by Euler's beam bending equation.
- Overall fastener preloads as indicated by assembly using Grade 2 and Grade 5 torques were repeatable. The tighter joints yielded a 2-3% increase in natural frequency
- Inherent part-to-part variation in natural frequency estimates varied by 2-4% for individual weldments. Assembly-to-assembly beams varied by 3-7% for natural frequencies. These are not measurement uncertainties, but rather product behavior variations.
- Natural frequency variation roughly increased linearly with the nominal frequency of the modes. Since the spacing of FRF spectral lines is not logarithmic, this means that low frequency modes will vary across fewer spectral lines than higher modes.
- Inherent part-to-part variation in damping values were 35% for individual simple weldments, and as large as 111% percent for assemblies. These are not measurement uncertainties, but rather product behavior variations.
- Assuming surface finish quality and fastener preload deteriorate as an assembly ages, the natural frequencies will become lower and the damping values will become higher for worn products.
- Given the product behavior variations found among a relatively few beam assemblies, the consumer of damping data is cautioned to consider the potential impact of part-to-part variation on their analyses. Efforts spent while tuning models to closely emulate single-unit test data may be better spent quantifying product behavior variability.

APPENDIX: Log-Decrement calculations

Several steps were applied to the data for the log-decrement analysis, illustrated in the figures A1-A3:

(1) Bandpass filter five response decay traces (3-pole Butterworth between nominally 66% to 133% of resonance)

(2) Discard all data points that aren't peaks or valleys

(3) Divide every peak value by the subsequent peak, divide every valley by the subsequent valley. This yields a trace of "rebound" coefficients. Average several hundred such consecutive rebound values that don't appear victim to excessive round-off error.

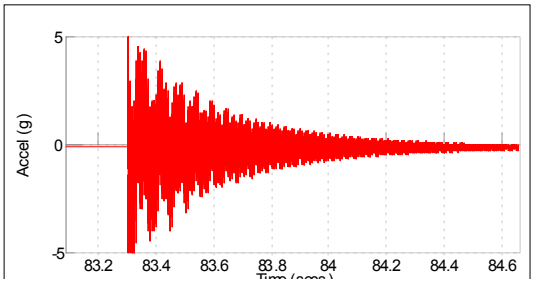

Figure A1. Raw accel. response to impact.

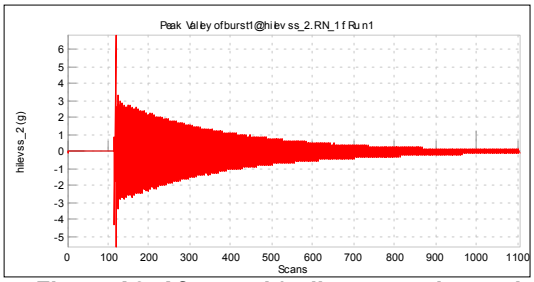

Figure A2. After peak/valley extraction and bandpass filter.

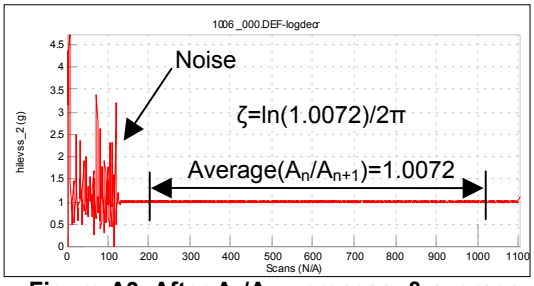

Figure A3. After A_n/A_{n+1} process, & average.

REFERENCES

[1] Hay, J., Blew, J., "Dynamic Testing and Computer Analysis of Automotive Frames," SAE Paper 720046, Society of Automotive Engineers, p.19, Jan. 1972.

[2] Riding, D., Weeks, R., "The Application of Noise Simulation Techniques to Conceptual Automotive Powertrain Design," SAE Paper 911077, Society of Automotive Engineers, p.3, 1991.

[3] Przybylinski, P.G., Anderson, G.B., "Engineering Data Characterizing the Fleet of U.S. Railway Rolling Stock, Volume II: Methodology and Data," FRA/ORD-81/75.2, DOT-TSC-FRA-81-16, II, Federal Railroad Administration, pg. 2-57, Nov. 1981.

[4] Cornwell, P., Farrar, C., Doebling, S., Sohn, H., “Environmental Variability of Modal Parameters,” *Experimental Techniques*, Vol. 23, No. 6, p.48, Nov./Dec. 1999.

[5] Kompella, M., Bernhard, R., “Variation of structural –acoustic characteristics of automotive vehicles,” Noise Control Engineering Journal, Vol. 44, No. 2, p. 93, Mar.-Apr. 1996.

[6] Marwala, T., Hunt, H., “Is Damage Identification Using Vibration Data in a Population of Cylinders Possible?” *Journal of Sound and Vibration*, Letters to the Editor, 237(4), p. 730, 2000.

[7] Chen, G., Yang, X., Mu, H., Nanni, A., “Destructive and Non-Destructive Testing of Bridge J857 Phelps County, Missouri,” Volume II, Report RDT01-002B, Missouri Dept. of Transportation, p.14, April, 2000.

[8] Lyon, R., “Variability in Response of Nominally Identical Structures,” 41st Meeting of the MFPT Society, Winchester, VA, p.112.

[9] Migeot, J., Coyette, J., Meerbergen, K., “Predicting Car Body Dynamics at Higher Frequencies: Challenges and Possible Solutions,” accessed via internet (jean-louis.migeot@fft.be), Free Field Technologies, Summer 2003.

[10] Dossing, O., “Dynamic Design Verification of a Prototype Rapid Transit Trains using Modal Analysis,” Bruel & Kjaer Application Note, copy obtained 1986.

[11] McClelland, W., Hay, J., Klosterman, A., “Frame Design Analysis Under Complete Vehicle Boundary Conditions,” SAE Paper 741142, Society of Automotive Engineers, p.17, Nov. 1974.

[12] Stein, P., “Experiment No. 6, The Response of Transducers to the Environemnt. The Problem of Signal and Noise,” Lf/MSE Publ. No. 38, Fall, 1971, Stein Measurement Services, Phoenix, AZ, p. 14.

[13] Vold, H., Morrow, D., “Compression of Time Histories Used for Component Fatigue Evaluation,” SAE Paper 930403, Society of Automotive Engineers, 1993.

[14] ISO-2631, “Mechanical vibration and shock – Evaluation of human exposure to whole-body vibration,” International Organization for Standardization, Technical Committee ISO/TC 108, Second Edition 1997-05-01.

[15] Gaberson, H.A., and Chalmers, R.H., "Modal Velocity as a Criterion of Shock Severity," Shock & Vibration Bulletin 40:2, US Naval Research Laboratory, Washington, DC, 1969.

[16] Timoshenko, S.P., *Vibration Problems in Engineering, 3rd Ed.*, D. Van Nostrand Inc., Princeton, NJ, 1955.

[17] Crandall, S.H., "Relation Between Strain and Velocity in Resonant Vibration," Journal of Acoustic Society of America Vol. 34 No. 12, 1962.

[18] Harris, C.M., and Batchelor, C., *Shock and Vibration Handbook, 4th Ed.*, McGraw-Hill Inc., New York, NY, 1996.

[19] Shigley, J.E., and Mischke, C.R., *Mechanical Engineering Design, 5th Ed.*, McGraw-Hill Inc., New York, NY, 1989.

[20] Thomson, W.T., and Dahleh, M.D., *Theory of Vibration with Applications, 5th Ed.*, Prentice Hall Inc., Upper Saddle River, NJ, 1993.

[21] Beckwith, T., Buck, N., “Mechanical Measurements,” 2nd Edition, Addison-Wesley, Reading, Mass., p.151, June 1973.

[22] Smith, K., Shust, W., “Bounding Natural Frequencies in Structures I: Gross Geometry, Material, and Boundary Conditions,” Proceedings of the XXII International Modal Analysis Conference, Society of Experimental Mechanics, 2004.